Journal of Materials Science: Materials in Electronics (2018) 29:19393–19401
https://doi.org/10.1007/s10854-018-0068-z

Template-free synthesis of uniform rose-like MoS_2 hierarchitectures and their enhanced photocatalytic properties

Huijie Wu[1] · Yuan Li[2,3]

Received: 26 June 2018 / Accepted: 17 September 2018 / Published online: 21 September 2018

Abstract
In this work, uniform rose-like MoS_2 hierarchitectures have been succefully synthesized on a large scale through a template-free hydrothermal method by the reaction of hexaammonium heptamolybdate tetrahydrate [$(NH_4)_6Mo_7O_{24}{\cdot}4H_2O$] and thioacetamide ($CH_3CSNH_2$). The rose-like MoS_2 hierarchitectures have a diameter of 350–450 nm and are formed by the assembly of numerous nanosheets. A reasonable growth mechanism of the MoS_2 hierarchitectures was proposed according to the time-dependent experiments. In addition, the as-prepared rose-like MoS_2 hierarchitectures show a large specific surface area of 33.72 $m^2\ g^{-1}$ with a dominant pore diameter of 46 nm. UV–Vis absorption spectrum indicated that the sample shows a large blue-shift compared to bulk MoS_2. The photocatalytic properties were investigated and exhibit enhanced visible light photocatalytic performance with the assistence of H_2O_2, which can be attributed to the special structural feature with an open and porous nanostructured surface layer that significantly facilitates the diffusion and mass transportation of MB molecules and oxygen species in photochemical reaction of MB degradation. This resulting rose-like MoS_2 hierarchitectures are very promising visible light photocatalysts for the degradation of dye pollutants and other applications.

1 Introduction

As an important transition-metal dichalcogenide semiconductor, molybdenum disulfide (MoS_2) has a unique anisotropic layered molecule structure constructed by stacking covalently bound S–Mo–S through weak van der Waals interactions, which has been receiving considerable attention due to its excellent optical properties, superior electrical performance and robust mechanical properties for fundamental studies and potential applications [1, 2]. In recent years, it has been extensively studied in different fields, such as lubricant [3], hydrogen evolution reactions [4], lithium ion batteries [5, 6], supercapacitors [6, 7], photoluminescence [8], transistors [9], sensing [10], and catalysis [11–13].

In addition, the properties of semiconductor nanocrystals depend greatly on their shape, size and hierarchy, so controlling the architecture of semiconductor nanocrystals has attracted much research interests [14, 15]. With the intention to prepare MoS_2 nanocrystals with desirable architectures, several synthesis approaches have been developed, such as hydrothermal method [16], solvothermal method [17], chemical vapor deposition method [18], electrospinning [19] and electrochemical exfoliation [20]. To date, MoS_2 with various morphologies including nanospheres, nanoplates, nanowires, nanorods, nanotubes and nanoflowers have been prepared. However, most of these approaches require templates or surfactants, complicated process control, as well as inhomogeneity in morphology/size of the product. Therefore, it is still a great challenge to controllably synthesize MoS_2 hierarchitectures with homogenous and well-defined morphologies via facile routes.

Herein, we demonstrate a facile and template-free hydrothermal route to prepare uniform rose-like MoS_2 hierarchitectures on a large scale. To the best of our knowledge, uniform rose-like MoS_2 hierarchitectures with enhanced visible light photocatalytic properties were rarely reported. The structure, morphology, formation mechanism, optical

✉ Yuan Li
liyuansjtu@swu.edu.cn

[1] Research Institute for New Materials Technology, Chongqing University of Arts and Sciences, Chongqing 400715, People's Republic of China

[2] Institute for Clean energy & Advanced Materials, Faculty of Materials & Energy, Southwest University, Chongqing 400715, People's Republic of China

[3] Chongqing Key Laboratory for Advanced Materials and Technologies of Clean Energies, Chongqing 400715, People's Republic of China

absorption property and photocatalytic activity of the as-prepared MoS_2 hierarchitectures are explored in detail.

2 Experimental section

2.1 Preparation of uniform rose-like MoS_2 hierarchitectures

All the chemical reagents in this experiment were of analytical grade and used without further purifiation. The typical synthesis was as follows. Firstly, 1 mmol $(NH_4)_6Mo_7O_{24}{\cdot}4H_2O$ and 10 mmol CH_3CSNH_2 (TAA) were dissolved in 40 ml distilled water under vigorous stirring for 30 min to form a transparent solution. Secondly, the solution was transferred into a 50 ml Teflon-lined stainless steel autoclave and sealed tightly. Thirdly, the autoclave was heated at 220 °C for 20 h in an oven and the resulting black product was collected by centrifugation. Finally, the as-prepared sample was washed several times with distilled water and absolute ethanol, and dried in a vacuum oven at 50 °C for 6 h.

2.2 Photocatalytic activity

The photocatalytic activity of the sample was compared by monitoring the discoloration of MB dye under visible light irradiation. In a typical process, 10 mg catalyst (MoS_2, Degussa P25 TiO_2) was added into a quartz tube containing a MB dye solution (100 ml, 20 mg l^{-1}), which was placed with a 15 cm distance from the lamp. Then 0.5 ml H_2O_2 (30%, w/w) was added into the solution. Prior to the illumination, the mixture was then placed in an ultrasonic water bath for 15 min, followed by magnetically stirring in the dark at ambient temperature for 30 min to achieve the adsorption–desorption equilibrium. Afterwards, the quartz tube was exposed to the visible ligh irradiation produced by a 150 W Xe arc lamp equipped with a UV cut off filter ($\lambda > 420$ nm). At given time intervals, 3 ml of suspension was sampled and centrifuged, and the supernatant was collected for absorption analysis on a UV–Vis spectrophotometer. The absorbance of MB at 664 nm was used for measuring the residual dye concentration.

2.3 Characterization techniques

The crystalline phase was analyzed by X-ray diffractometer (XRD, D/Max-IIIA X-ray, Cu-Kα: $\lambda = 1.54056$ Å) at a scanning rate of 0.04° S^{-1} from 10° to 90°. The composition was further analyzed by X-ray photoelectron spectroscopy (XPS) spectrum on a thermo ESCALAB 250 electron spectrometer with a monochromatic Al Kα X-ray source and a charge neutralizer. The morphology and crystal structure were performed by field emission scanning electron microscope (FEI Nova 400 SEM), transmission electron microscope (TEM, JEOL 2011) and high resolution TEM (HRTEM). The specific surface area and pore size distribution were obtained from the N_2 adsorption–desorption isotherm measured by Brunaur–Emmett–Teller (BET) surface analyzer (NOVOE 4000). The optical absorption properties were determined by UV–Vis spectrophotometer (Hitachi model U-3310).

3 Results and discussion

The XRD pattern of the product synthesized at 220 °C for 20 h is shown in Fig. 1. All the diffraction peaks can be well indexed to the corresponding hexagonal phase of MoS_2 (JCPDS card no. 37-1492) with lattice constants of $a = 3.161$ Å and $c = 12.84$ Å. The strong diffraction peaks at 14.35°, 32.67° and 60.12° correspond to the respective (002), (100) and (008) planes of the hexagonal phase of MoS_2. No other characteristic peaks of impurities are observed, indicating that the sample was highly crystalline.

The as-prepared sample was characterized by XPS to investigate the composition and purity. Figure 2a shows the XPS survey spectrum of as-synthesized MoS_2. Based on peaks due to the binding energies, the elements in the compound are established. The sample is composed of two major elements of Mo and S, and a trace amount of C and O. As shown in Fig. 2b, the peaks at 228.8 and 232.1 eV are respectively associated with Mo^{4+} $3d_{3/2}$ and Mo^{4+} $3d_{5/2}$ [21], and those at 234.1 and 235.8 eV should be ascribed to Mo^{6+}, which might be originated from the slight surface oxidation of MoS_2 in air and it was also observed in the S 2*p* region of the spectrum [22]. Additionally, we did not find any MoO_3 in XRD and HRTEM images. Previous reports

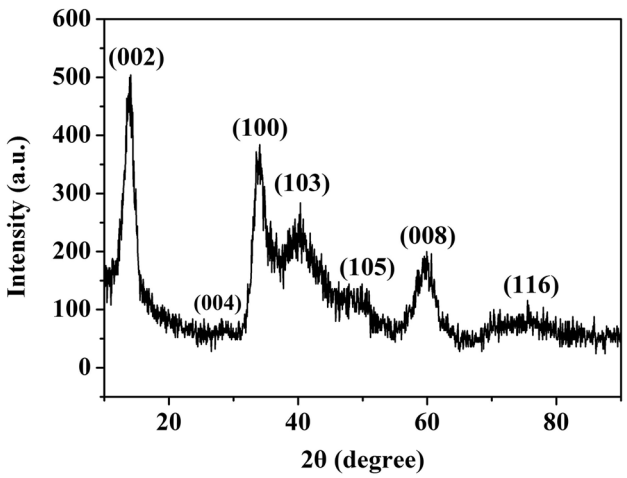

Fig. 1 XRD pattern of the product obtained at 220 °C for 20 h

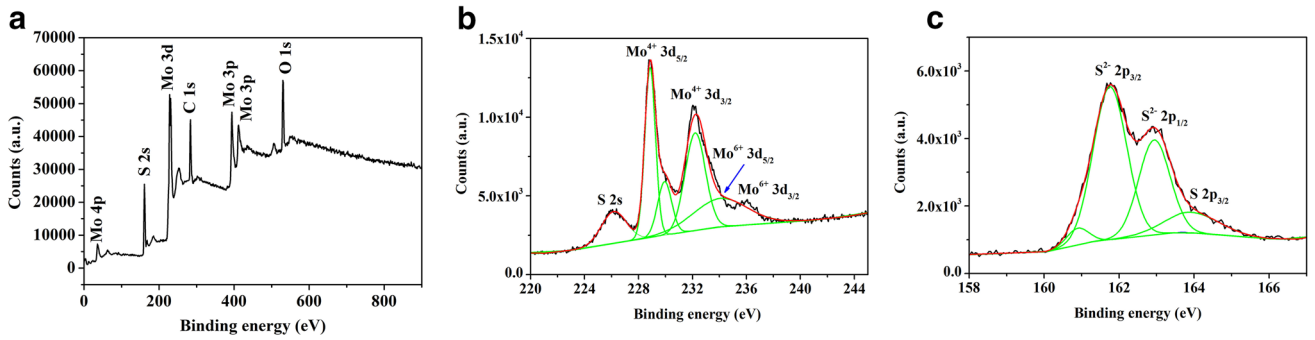

Fig. 2 XPS spectrum of the product obtained at 220 °C for 20 h

indicate that the defects and edges of MoS_2 are highly reactive with oxygen, so some oxygen is likely bonded to defects and edges of the MoS_2 nanosheets [23]. The peaks at 161.7 and 162.9 eV (Fig. 2c) are respectively attributed to S $2p_{3/2}$ and S $2p_{1/2}$ of divalent sulfide ions (S^{2-}), while the peak at 163.8 eV for S_2^{2-} indicate the presence of bridging S_2^{2-} or apical S^{2-} resulting from the unsaturated S atoms on the top and bottom of S–Mo–S layers [24, 25].

The typical SEM images of the obtained sample are shown in Fig. 3a, b. They are composed of uniform rose-like MoS_2 hierarchitectures approximately 350–450 nm in diameter. A high-magnification SEM image (Fig. 3c) reveals that the rose-like MoS_2 hierarchitectures have open and porous nanostructured surface layers, which are built of many thin nanosheets. An enlarged SEM image of an individual rose-like MoS_2 hierarchitecture (Fig. 3d) clearly exhibits that the nanosheets with a thickness of only about 2–5 nm stretch out towards the edge of the nanoflowers, and connect to each other to form the rose-like hierarchitectures.

The TEM images (Fig. 4a, b) further confirm the rose-like hierarchitectures, and nanosheets are self-assembled to form rose-like hierarchitectures. The selected area electron diffraction (SAED) pattern (Fig. 4c) exhibits five sharp rings from (002), (004), (100), (103) and (105) planes of hexagonal phase MoS_2, implying its polycrystalline nature. The HRTEM image (Fig. 4d) taken from nanosheets is clearly visible, with a spacing of 0.62 nm, corresponding to the spacing of the (002) plane of hexagonal phase MoS_2, which is in good agreement with the XRD result.

According to the previous reports [26, 27], the reaction process for the formation of MoS_2 rose-like hierarchitectures in the system consists of three steps: (1) formation of H_2S through the hydrolysis of thioacetamide. (2) Production of Mo (IV) by reduction of Mo (VI). (3) Formation of MoS_2. The process can be described as follows:

$$CH_3CSNH_2 + 2H2O \rightarrow CH_3COOH + NH_3 + H_2S \quad (1)$$

$$(NH_4)_6Mo_7O_{24} \cdot 4H_2O \rightarrow 7MoO_3 + 6NH_3 + 7H_2O \quad (2)$$

$$MoO_3 + 3H_2S + H_2O \rightarrow MoO_2 + SO_4^{2-} + 2H^+ \quad (3)$$

$$MoO_2 + 2H_2S \rightarrow MoS_2 + 2H_2O \quad (4)$$

To investigate the formation mechanism of rose-like MoS_2 hierarchitectures in detail, time-dependent experiments were carried out while keeping other reaction parameters constant. At the early growth stage (5 h), the product was composed of aggregated nanosheets (Fig. 5a). After 10 h, a great number of nanosheets began to assemble together resulting in the scabbled flower-like morphology, but there still existed a few nanosheets (Fig. 5b). 15 h later, no nanosheets remained and the product was loose flowers with the diameter of about 250–350 nm (Fig. 5c). As the reaction time was prolonged to 20 h, uniform rose-like MoS_2 hierarchitectures with larger size formed (Fig. 5d).

On the basis of the above experimental results, a proposed formation mechanism of rose-like MoS_2 hierarchitectures is suggested, as shown in Scheme 1. (1) Initial nucleating: firstly, according to the equations, $(NH_4)_6Mo_7O_{24}{\cdot}4H_2O$ reacts with TAA forming MoS_2 nuclei rapidly in the supersaturated solution. Then MoS_2 nuclei begin to grow into primary nanosheets according to their crystal growth habit (oriented growth with two-dimensional direction) [28]. (2) Driven by the minimization of overall surface energy, the MoS_2 nanocrystals have a tendency to orient aggregation, through the attachment among the primary nanosheets [29]. (3) These loose and scabbled flower-like structures undergo restructuring or rearranging into a more compact texture, and well-defined rose-like MoS_2 hierarchitectures formed through the Ostwald ripening process [30].

The specific surface area and pore size distribution of the as-synthesized rose-like MoS_2 hierarchitectures were tested by nitrogen adsorption–desorption (Fig. 6a). The Brunauer–Emmett–Teller (BET) surface area of rose-like MoS_2 hierarchitectures was calculated to be 32.72 $m^2\ g^{-1}$ and a total pore volume of 0.157 $cm^3\ g^{-1}$. This is a very high surface area for MoS_2 flower-like structures. Such a surface area value is larger than the MoS_2 nanoflowers reported by

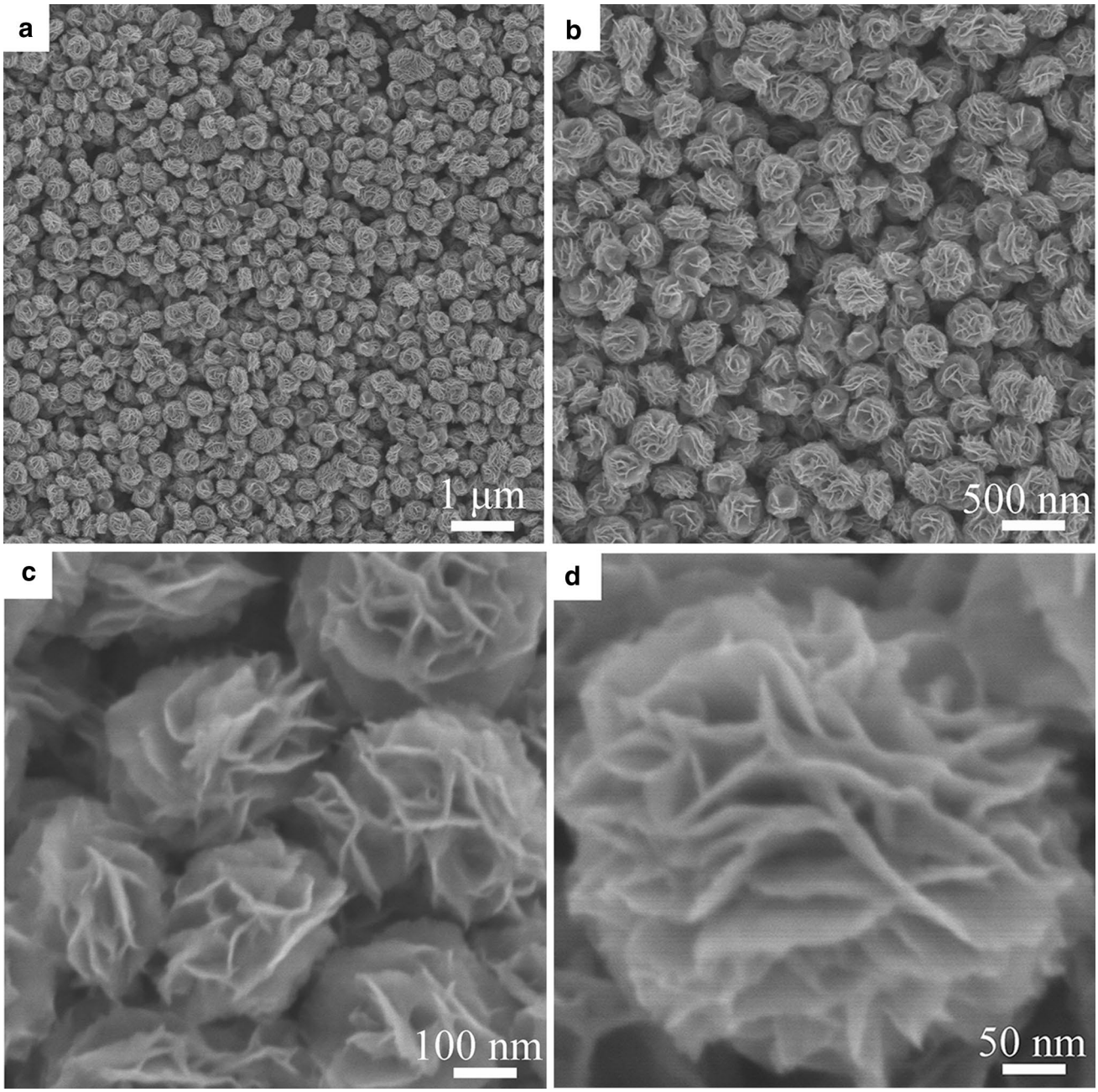

Fig. 3 FESEM images of the as-prepared rose-like MoS_2 hierarchitectures: **a** and **b** low-magnification SEM images; **c** high-magnification SEM image; **d** enlarged SEM image of an individual rose-like MoS_2 hierarchitecture

Gao [31]. The average pore diameter is 46 nm obtained by the Barrett–Joyner–Halenda (BJH) method (Fig. 6b).

The optical absorption property of the as-synthesized rose-like MoS_2 hierarchitectures was investigated at room temperature by UV–Vis spectroscopy (Fig. 7a). Two absorption peaks at 620 and 490 nm in the visible light region are assigned to the direct excitonic transition at the K point of the Brillouin zone, which is represented by a blue-shift that reveals changes in the direct transitions from the valence band to the conduction band above the valence gap [32]. The band gap energy of direct gap semiconductor rose-like MoS_2 hierarchitectures is calculated by the below equation [33].

$$(\alpha h\upsilon)^2 = A\left(h\nu - E_g\right) \tag{5}$$

where α is the absorption coefficient, $h\nu$ is the photon energy, A is a constant, and E_g is the band gap. To calculate the band gap energy, $(\alpha h\nu)^2$ versus $h\nu$ curve was plotted

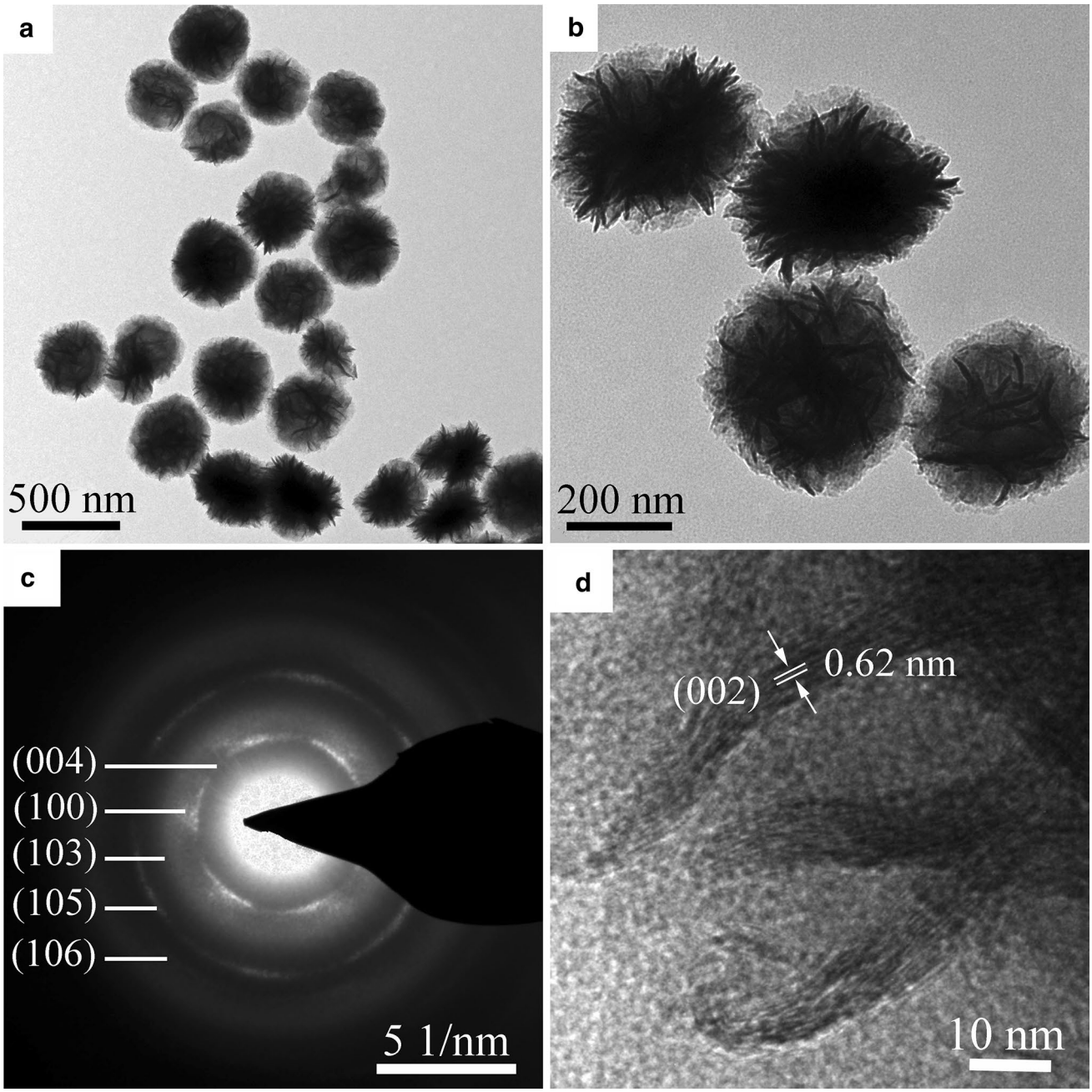

Fig. 4 Typical TEM images of the as-prepared rose-like MoS_2 hierarchitectures: **a** low-magnification TEM image; **b** high-magnification TEM image; **c** corresponding SAED pattern of the rose-like MoS_2 hierarchitectures; **d** HRTEM image of the rose-like MoS_2 hierarchitectures

(Fig. 7b). According to the above equation, the optical band gap energy of the rose-like MoS_2 hierarchitectures is estimated to be 2.75 eV, which indicated that the as-prepared MoS_2 is suitable for visible light photocatalyst. Compared with bulk MoS_2, which has an absorption edges at 1040 nm (1.23 eV band gap) [34], the as-prepared rose-like MoS_2 hierarchitectures (2.75 eV band gap) exhibits a large blue-shift, presumably attributing to the strong quantum confinement effect [35]. In general, the band gap of nano-MoS_2 increases due to the quantum effect and its redox potentials are accordingly changed. The appropriate alternation in the energy levels of the conduction and valence band edges allow MoS_2 nanomaterials to act as photocatalysis.

To further understand the photocatalytic process, the possible photocatalytic mechanism of MoS_2 was presented, as shown in Scheme 2. When a semiconductor photocatalyst is illuminated by light, the activated electron excited from valence band (VB) is transferred to conduction band (CB)

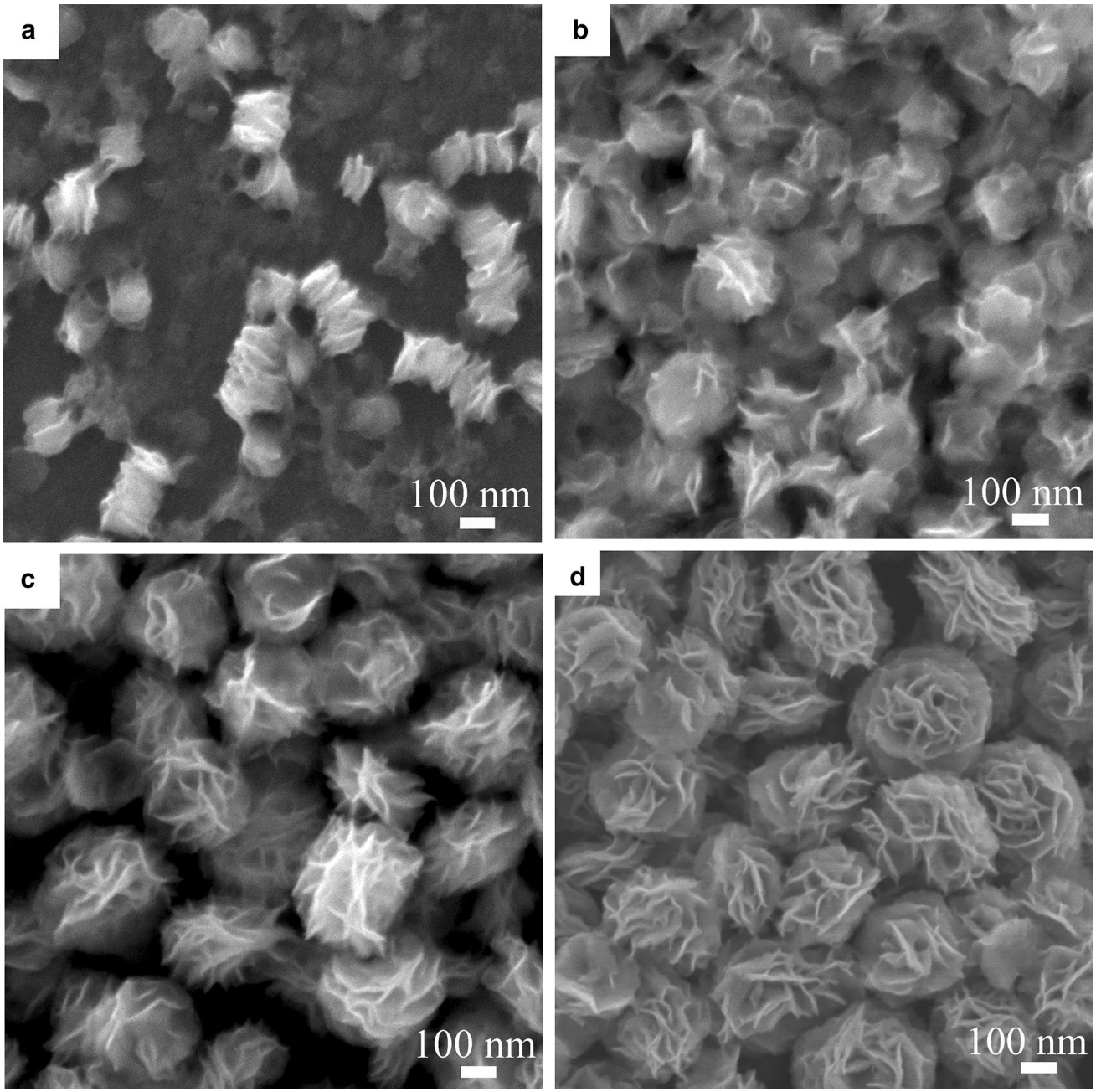

Fig. 5 The evolution process of the rose-like MoS_2 hierarchitectures monitored by FESEM technique: **a** 5 h; **b** 10 h; **c** 15 h; **d** 20 h

by creating holes in the valence band. These charge carriers will recombine quickly and forms photoexcited electron–hole (e^-/h^+) pairs. These photoexcited charge carriers may either recombine or absorbed by other species such as oxygen or water by forming reactive oxygen species such as hydroxyl and superoxide radical anions. Hydrogen peroxide (H_2O_2) as a scavenger can prevent the recombination of the photo-generated e^-/h^+ pairs and improve the photocatalytic properties by capturing the photo-generated e^-/h^+ pairs, resulting in the formation of oxidant species OH [36]. Then these photoinduced holes react with H_2O to produce hydroxyl radicals ($^{\cdot}OH$) or permit direct oxidation of MB dye to reactive intermediate, while electrons react with O_2 to form superoxide radical anions ($^{\cdot}O_2^-$) [37]. These formed radicals will break and destroy the various pollutants into small colourless molecules [38]. The possible mechanisms for the photocatalytic degradation of MB dye can be as follows:

$$MoS_2 + h\nu \rightarrow e^- + h^+ \quad (6)$$

$$e^- + H_2O_2 \rightarrow {}^{\cdot}OH + OH^- \quad (7)$$

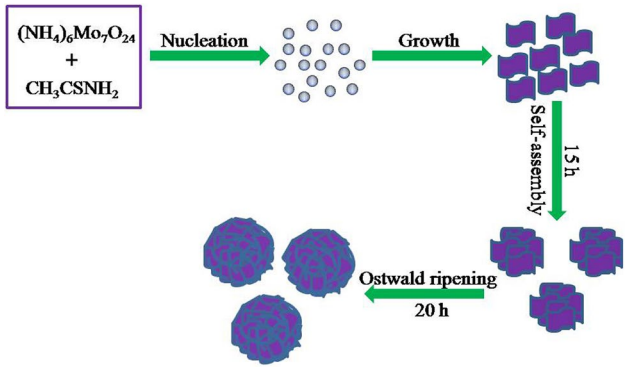

Scheme 1 Schematic illustration of the formation of the rose-like MoS_2 hierarchitectures

$$h^+ + H_2O_2 \rightarrow H^+ + {}^{\cdot}OOH \quad (8)$$

$${}^{\cdot}OOH + H_2O_2 \rightarrow {}^{\cdot}OH + H_2O + O_2 \quad (9)$$

$$h^+ + H_2O \rightarrow {}^{\cdot}OH + H^+ \quad (10)$$

$$e^- + O_2 \rightarrow {}^{\cdot}O_2^- \quad (11)$$

$$h^+ + MB \rightarrow MB^{\cdot +} \rightarrow \text{final product} \quad (12)$$

$${}^{\cdot}OH + MB \rightarrow MB^{\cdot} \rightarrow \text{final product} \quad (13)$$

To establish the potentiality of the as-synthesized rose-like MoS_2 hierarchitectures in the discoloration of organic contaminants, we have investigated their photocatalytic activities by choosing the photocatalytic discoloration of MB

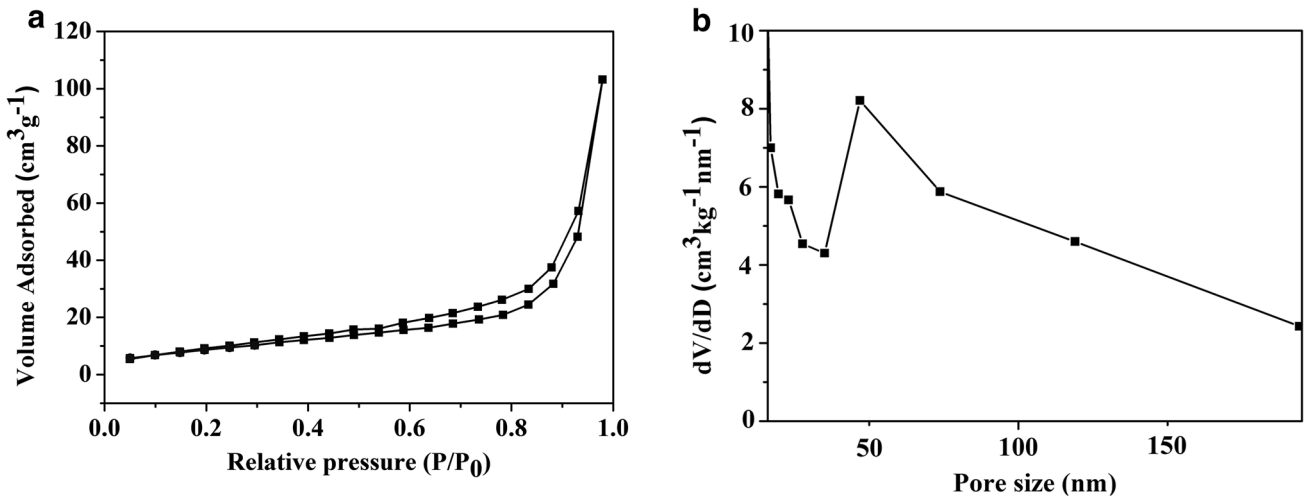

Fig. 6 **a** N_2 adsorption–desorption isotherm of the rose-like MoS_2 hierarchitectures; **b** the pore size distribution

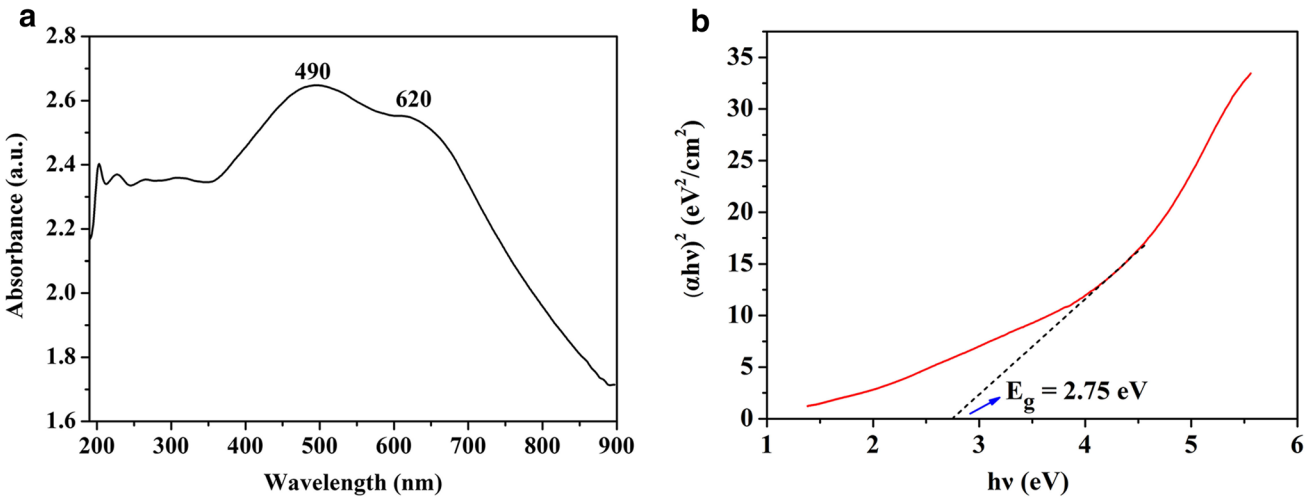

Fig. 7 **a** UV–Vis absorption spectrum of the rose-like MoS_2 hierarchitectures; **b** band gap spectrum of the rose-like MoS_2 hierarchitectures

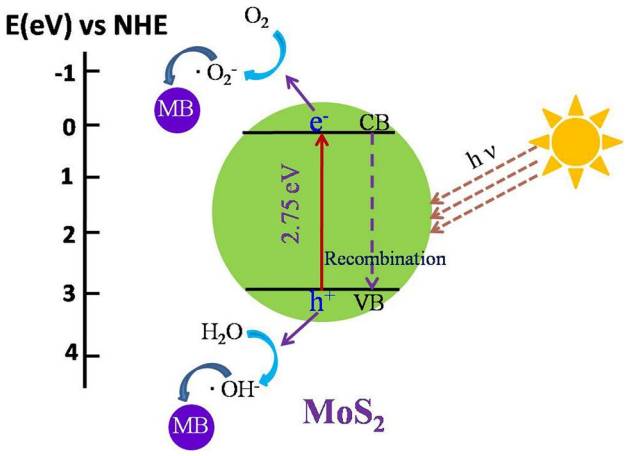

Scheme 2 The photocatalytic mechanism of MoS_2 photocatalyst to MB under visible light irradiation

in the presence of H_2O_2. Figure 8a shows temporal evolution of the absorption spectra of MB aqueous solution in the presence of rose-like MoS_2 hierarchitectures under visible light irradiation. The strength of characteristic peak for MB decreases after the simulated visible light irradiation. The color of the dye solution changes from its initial deep blue to a light blue, and then to transparent, which can be observed by naked eyes. These results indicate the decomposition of MB. From Fig. 8b, it is found that in the presence of MoS_2 catalyst and H_2O_2, MB discolours dramatically up to 94% after 120 min visible light irradiation. It should be noted that the degradation rate of MoS_2 rose-like hierarchitectures with the assistance of H_2O_2 is superior to the reported value in the literature [11]. The blank experiment with catalyst absence also has been performed. There is only 11% degradation efficiency of MB under the same irradiation time, implying the significant role of MoS_2 played in the photocatalytic degradation of MB. In the presence of only MoS_2 catalyst without H_2O_2, MB discolours up to 54%. In addition, under the same experimental conditions, the photocatalytic activity of commercial photacatalyst Degussa P25 TiO_2 was also measured. It can be clearly observed that there is only 14% degradation of MB under the same irradiation time, indicating the higher visible light photocatalytic properties of the as-prepared rose-like MoS_2 hierarchitectures.

To further investigate the stability and recyclability properties of MoS_2 catalyst, it has been tested by repeating the degradation process of the MoS_2 photocatalyst. After each cycle, the MoS_2 catalyst can be easily separated by centrifugation and reused for its catalytic property. Figure 8c shows recycling photocatalytic degradation of MB in the presence of rose-like MoS_2 hierarchitectures and H_2O_2 under visible light irradiation. It can be clearly seen that the degradation rate of MB dye was almost 90% in each cycle and the small decrease in the degradation rate after five cycles is probably due to materials loss during the washing process. The results of five repeated experiments show that the MoS_2 photocatalyst is stable and recyclable under visible light irradiation.

4 Conclusion

A facile and template-free hydrothermal method has been successfully developed to fabricate uniform rose-like MoS_2 hierarchitectures. The UV–Vis absorption spectrum of the as-prepared rose-like MoS_2 hierarchitectures exhibits a large blue-shift in the band gap energy compared to bulk MoS_2. The enhanced photocatalytic activity for the MB degradation is obtained on rose-like MoS_2 hierarchitectures and the recycling test displays that the photocatalytic activity is stable. Such tailored rose-like MoS_2 hierarchitectures would be expected to have more potential applications in the filed of photocatalytic decomposition pollutants.

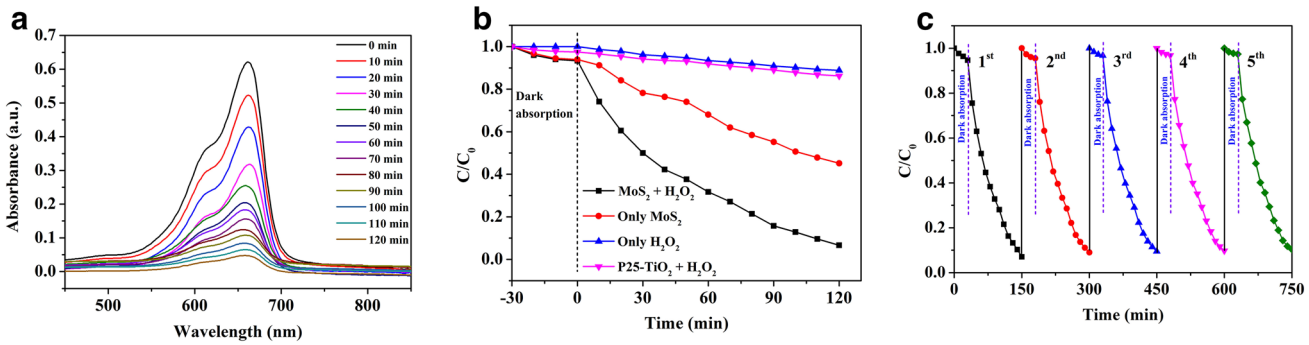

Fig. 8 **a** Temporal evolutions of absorption spectrum for MB aqueous solutions in the presence of rose-like MoS_2 hierarchitectures and H_2O_2 under visible light irradiation; **b** plots of the degradation rate of MB in aqueous solution against specific time intervals under various conditions; **c** recycling photocatalytic degradation of MB in the presence of rose-like MoS_2 hierarchitectures and H_2O_2 under visible light irradiation

Acknowledgements This work was supported by the Fundamental Research Funds for the Central Universities (Project Nos. XDJK2016C003, XDJK2017C003; XDJK2016E001, for Innovation and Entrepreneurship Students), the Foundation of Chongqing Municipal Education Commission (Grant Nos. KJ1711292; KJ1711272), Chongqing Natural Science Foundation (Grant Nos. cstc2016shmszx20002; cstc2016jcyjA0140; cstc2017jcyjA1821), Chongqing university outstanding achievement transformation projects (Grant No. KJZH17130), and Funding scheme for youth backbone teachers of universities in Chongqing.

Compliance with ethical standards

Conflict of interest The authors declare that there is no conflict of interests regarding the publication of this paper.

References

1. N. Goswami, A. Giri, S.K. Pal, Langmuir **29**, 11471 (2013)
2. S.Z. Butler, S.M. Hollen, L.Y. Cao et al., ACS Nano **7**, 2898 (2013)
3. Z. Li, J. Wang, J. Lu, J. Meng, Appl. Surf. Sci. **264**, 516 (2013)
4. B.J. Guo, K. Yu, H.L. Li et al., ACS Appl. Mater. Interfaces **8**, 5517 (2016)
5. T. Yang, Y.J. Chen, B.H. Qu et al., Electrochim. Acta **115**, 165 (2014)
6. Z.C. Wu, B. Li, Y.J. Xue, J.J. Li, Y.L. Zhang, F. Gao, J. Mater. Chem. A **3**, 19445 (2015)
7. X.P. Zhou, B. Xu, Z.F. Lin, D. Shu, L. Ma, J. Nanosci. Nanotech. **14**, 7250 (2014)
8. G. Eda, H. Yamaguchi, D. Voiry, T. Fujita, M. Chen, M. Chhowalla, Nano Lett. **11**, 5111 (2011)
9. D.J. Late, B. Liu, H.S.S.R. Matte, V.P. Dravid, C.N.R. Rao, ACS Nano **6**, 5635 (2012)
10. X.X. Wang, F.X. Nan, J.L. Zhao, T. Yang, T. Ge, K. Jiao, Biosens. Bioelectron. **64**, 386 (2015)
11. Z.H. Zhou, Y.L. Lin, P.G. Zhang, Mater. Lett. **131**, 122 (2014)
12. H. Zhu, M.L. Du, M. Zhang, M.L. Zou, T.T. Yang, Y.Q. Fu, J.M. Yao, J. Mater. Chem. A **2**, 7680 (2014)
13. Y.Y. Zhao, L. Kuai, Y.G. Liu et al., Sci. Rep. **5**, 8722 (2015)
14. R.W.J. Scott, M.J. MacLachlan, G.A. Ozin, Curr. Opin. Solid State Mater. Sci. **4**, 113 (1999)
15. P. Kar, S. Farsinezhad, X.J. Zhang, K. Shankar, Nanoscale **6**, 14305 (2014)
16. K.J. Huang, J.Z. Zhang, G.W. Shi, Y.M. Liu, Electrochim. Acta **132**, 397 (2014)
17. N. Berntsen, T. Gutjahr, L. Loeffler, J.R. Gomm, R. Seshadri, W. Tremel, Chem. Mater. **15**, 4498 (2003)
18. J. Etzkorn, H.A. Therese, F. Rocker, N. Zink, U. Kolb, Adv. Mater. **17**, 2372 (2005)
19. S.S. Liu, X.B. Zhang, H. Shao, J. Xu, F.Y. Chen, Y. Feng, Mater. Lett. **73**, 223 (2012)
20. N. Liu, P. Kim, J.H. Kim, J.H. Ye, S. Kim, C.J. Lee, ACS Nano **8**, 6902 (2014)
21. W.K. Ho, J.C. Yu, J. Lin, J.G. Yu, P.S. Li, Langmuir **20**, 5865 (2004)
22. Q.S. Gao, L.C. Yang, X.C. Lu, J.J. Mao, Y.H. Zhang, Y.P. Wu, Y. Tang, J. Mater. Chem. **20**, 2807 (2010)
23. S.M. Cui, Z.H. Wen, X.K. Huang, J.B. Chang, J.H. Chen, Small **11**, 2305 (2015)
24. Y. Yan, B.Y. Xia, X.M. Ge, Z.L. Liu, J.Y. Wang, X. Wang, ACS Appl. Mater. Interfaces **5**, 12794 (2013)
25. H. Vrubel, D. Merki, X. Hu, Energy Environ. Sci. **5**, 6136 (2012)
26. C. Feng, J. Ma, H. Li, R. Zeng, Z.P. Guo, H.K. Liu, Mater. Res. Bull **44**, 1811 (2009)
27. R.H. Barnsley, A.H. Thompson, Solid State Sci. **8**, 1133 (2006)
28. H. Liu, X. Su, C.Y. Duan, X.N. Dong, Z.F. Zhu, Mater. Lett. **122**, 182 (2014)
29. Y. Cheng, Y.S. Wang, Y.H. Zheng, Q. Yong, J. Phys. Chem. B **109**, 11548 (2005)
30. X.J. Dai, Y.S. Luo, S.Y. Fu, W.Q. Chen, Y. Lu, Solid State Sci. **12**, 637 (2010)
31. Y. Gao, C.L. Chen, X.L. Tan, H. Xu, K.R. Zhu, J. Colloid Interface Sci. **476**, 62 (2016) 62
32. S.K. Bhar, N. Mukherjee, S.K. Maji, B. Adhikary, A. Mondal, Mater. Res. Bull. **45**, 1948 (2010)
33. C. Yang, H. Fan, Y. Xi, J. Chen, Z. Li, Appl. Surf. Sci. **254**, 2685 (2008)
34. K.K. Kam, B.A. Parkinson, J. Phys. Chem. **86**, 463 (1982)
35. J.P. Wilcoxon, P.P. Newcomer, G.A. Samara, J. Appl. Phys. **81**, 7934 (1997)
36. A. Ghosh, C. Kulsi, D. Banerjee, A. Mondal, Appl. Surf. Sci. **369**, 525 (2016)
37. H. Zhang, X.F. Fan, X. Quan, S. Chen, H.T. Zu, Environ. Sci. Technol. **45**, 5731 (2011)
38. T. Oku, N. Kakuta, K. Kobayashi, A. Suzuki, K. Kikuchi, Prog. Nat. Sci. **21**, 122 (2011)